ISSN 1811-2382, Polymer Science, Series C, 2020, Vol. 62, No. 2, pp. 238–258. © Pleiades Publishing, Ltd., 2020.
Russian Text © The Author(s), 2020, published in Vysokomolekulyarnye Soedineniya, Seriya C, 2020, Vol. 62, No. 2, pp. 245–266.

Highly Permeable Polyheteroarylenes for Membrane Gas Separation: Recent Trends in Chemical Structure Design

A. Yu. Alent'ev[a],*, V. E. Ryzhikh[a], and N. A. Belov[a]

[a] *Topchiev Institute of Petrochemical Synthesis, Russian Academy of Sciences, Moscow, 119991 Russia*

**e-mail: alentiev@ips.ac.ru*

Received April 6, 2020; revised June 4, 2020; accepted June 27, 2020

Abstract—Progress in membrane gas separation is impossible without the synthesis of new polymers with improved gas-transport and gas-separation characteristics. The most promising polymeric membrane materials with the advantageous combination of permeability and selectivity, which form the 2008 and 2015 Robeson "upper bounds," are polyheteroarylenes, among which are ladder polybenzodioxanes, polymers of intrinsic microporosity (PIM), polyimides, polyamides, and polyisathines. Their specific feature is the presence of moieties in the chemical structure that in any way contribute to the loosened packing of polymer chains and the increase in gas-permeability coefficients. Among such macromolecular design elements are groups with main chain kinks or bulky substituents increasing the rotation barriers and rigidity of macrochains. A high gas permeability of the polyheteroarylenes under consideration is commonly combined with an increased selectivity for many gas pairs (e.g., O_2/N_2, CO_2/CH_4) primarily associated with a high diffusion selectivity, which suggests their chain packing order and makes it possible to call them polymeric molecular sieves.

DOI: 10.1134/S1811238220020010

INTRODUCTION

The separation of gas mixtures is one of the most rapidly progressing and knowledge-based fields of membrane technology. The majority of membrane gas-separation processes is implemented with the use of asymmetric or composite membranes having a thin (from several tens to several hundred nanometers) nonporous selective polymer layer [1]. The gas flow through a membrane is limited in this case by flow through a thin selective layer and is directly proportional to pressure difference and inversely proportional to membrane thickness:

$$J = P\Delta p/l, \quad (1)$$

where Δp is the pressure difference on a membrane, l is the thickness of the membrane (selective layer), and P is the gas-permeability coefficient for the material of the membrane selective layer. The permeability coefficient is usually expressed in extra-system Barrer units (1 Barrer = 10^{-10} cm^3(STP) cm/(cm^2 s cmHg)). The value of P for polymeric materials varies within three to eight orders depending on the nature of a polymer and a gas [1–3]. According to the solution–diffusion transport mechanism, at low pressures the value of P is determined by the diffusion coefficient D and the solubility coefficient S of the gas in a material:

$$P = DS \quad (2)$$

The solubility coefficient S determines the driving force of the process and represents the thermodynamic characteristic of permeability, whereas the diffusion coefficient D is the kinetic factor defining the mobility of a penetrating component in the membrane material.

An important factor characterizing the efficiency of the gas-separation process is the selectivity of separation of gases i and j:

$$\alpha_{ij} = P_i/P_j. \quad (3)$$

With allowance for expression (2) selectivity α_{ij} is determined by the product of diffusion selectivity $\alpha_{ij}^D = D_i/D_j$ by solubility selectivity $\alpha_{ij}^S = S_i/S_j$. For the separation of mixtures of noncondensable gases, such as H_2, He, N_2, O_2, CO_2, and CH_4, glassy amorphous polymers possessing a high diffusion selectivity are used as a selective layer material [2]. The use of thermally stable polymers, including polyheteroarylenes, for the separation of these mixtures makes it possible not only to ensure membrane integrity and workability at relatively small variations in process temperature but also to widen the temperature range of membrane-based gas separation applications.

The commercial application of membrane gas separation began in the 1970s with such low-permeable polymers, such as polysulfone and cellulose acetate [1–5] with $P(O_2) \sim 1$ Barrer [6]. However, in the late 1970s a gas-separation membrane based on a much more permeable glassy poly(vinyltrimethylsilane) (**PVTMS**) ($P(O_2) \sim 40$ Barrer) was created in our

Table 1. Parameters of Eq. (4) for the 1991, 2008, 2015 Robeson "upper bounds"

Gas pair	k, Barrer			N		
	1991	2008	2015	1991	2008	2015
O_2/N_2	389224	1396000	16700000	−5.800	−5.666	−5.700
CO_2/CH_4	1073700	5369140	22584000	−2.6264	−2.636	−2.401
H_2/N_2	52918	97650	1100000	−1.5275	−1.4841	−1.46
H_2/CH_4	18500	27200	195000	−1.2112	−1.107	−1.10

country [6]. The reason behind high permeability of this silicon-containing polymer is the reduced packing density of macromolecular chains related to the bulky side group $-SiMe_3$ [7]. Just these design elements of elementary unit became decisive in membrane materials science in the 1980s-1990s. At that time, even higher permeable polymers, for example, poly(trimethylsilylpropine) (**PTMSP**) with $P(O_2) \sim$ 4000–10000 Barrer, were synthesized, and to date other polyacetylenes with $P(O_2)$ reaching 19000 Barrer have been obtained [6, 7]. Most polyheteroarylenes exhibit much lower gas permeability coefficients. For the ease of analysis and consideration this class of amorphous glassy polymers may be conditionally divided in terms of oxygen permeability coefficient into barrier ($P(O_2) < 0.01$ Barrer), low-permeable ($0.01 < P(O_2) < 1$ Barrer), medium-permeable (common) ($1 < P(O_2) < 20$ Barrer), and highly permeable ($P(O_2) > 20$ Barrer). In this review, we will limit ourselves to the group of highly permeable polyheteroarylenes, in accordance with the above-mentioned classification, which were synthesized and investigated in the past decade.

ANALYSIS PRINCIPLES

An increase in the permeability of polymers is generally accompanied by a reduction in their selectivity [2, 3, 5, 8, 9]. Therefore, the potential efficiency of a material for gas separation is determined by position of the experimentally measured values of P and α for a polymer on permeability–selectivity diagrams (Robeson diagrams) relative to the empirical so-called "upper bound" [8–11]. The "upper bound" on Robeson diagrams is formed by polymers with the most advantageous combination of permeability and selectivity and is described by the power dependence

$$P_i = k\alpha_{ij}^n, \quad (4)$$

where k and n are constants for each of the given gas pair [8–11]. Its position on the Robeson diagrams changes with time [12], that is, with the set of data on the polymers studied by a given time (Table 1). Position of the 1991 "upper bound" on these diagrams was determined primarily by low-permeable and medium-permeable polyimides, vinyl and methacrylic polymers, and highly permeable polyacetylenes [8]. Later, new classes of polymers were examined, such as medium-permeable and highly permeable perfluorinated amorphous Teflons, highly selective polypyrroles, and low-permeable and medium-permeable polyimides based on hexafluoroisopropylidenediphthalic dianhydride (**6FDA**), which defined position of the 2008 "upper bound" [9]. The main design element of these polymers was the introduction of fluorinated groups into the structure of elementary unit which loosened chain packing due to an increase in the volume of substituents and a decrease in the energy of interchain interactions. At the beginning of the 21st century, P.M. Budd and N.B. McKeown synthesized first ladder polybenzodioxanes (PIMs, polymers of intrinsic microporosity) [13, 14], which owing to high permeability and selectivity were also among polymers determining position of the "upper bound" [9]. PIM-1 was the first polymer of intrinsic microporosity which was most promising for gas separation and which was most easily synthesized [13, 15]

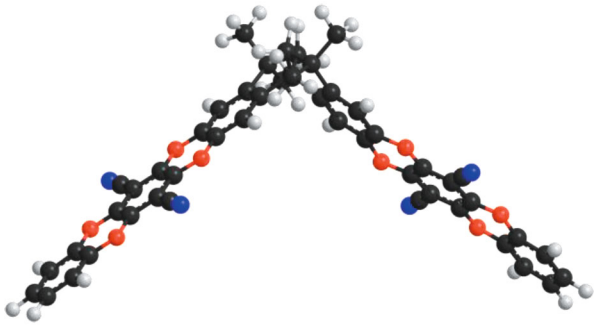

(hereinafter, carbon atoms are colored black, nitrogen atoms are colored blue, oxygen atoms are colored red, and hydrogen atoms are colored gray. Color figures are available in the electronic version of the journal).

The study of PIM-1 by computer simulation methods revealed that the reason behind high permeability and free volume is the presence of regular, almost rectangular, chain kinks related to the occurrence of a spirobis(indane) spacer at the site of connection of two five-membered cycles [16]. The rigid structure of the polymer with main chain kinks contributes to formation of the loose chain packing with a large free volume and a high internal surface area. Just this element of the molecular structure of the polymer chain, along

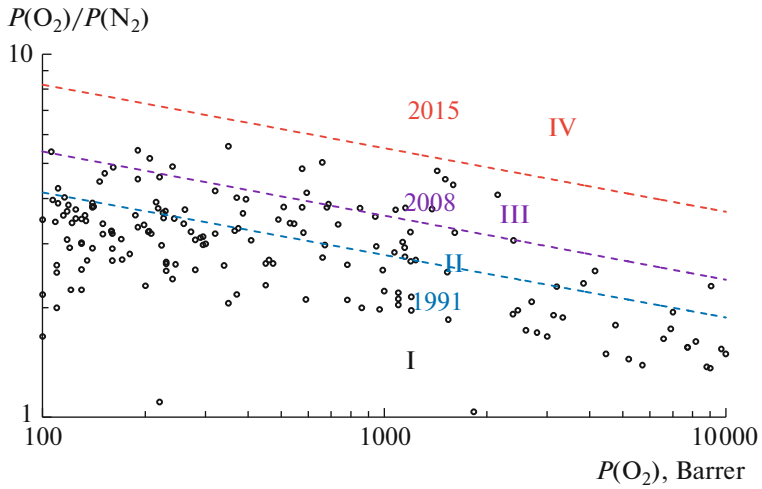

Fig. 1. Fragmented Robeson diagram for the gas pair oxygen/nitrogen. See text for explanations.

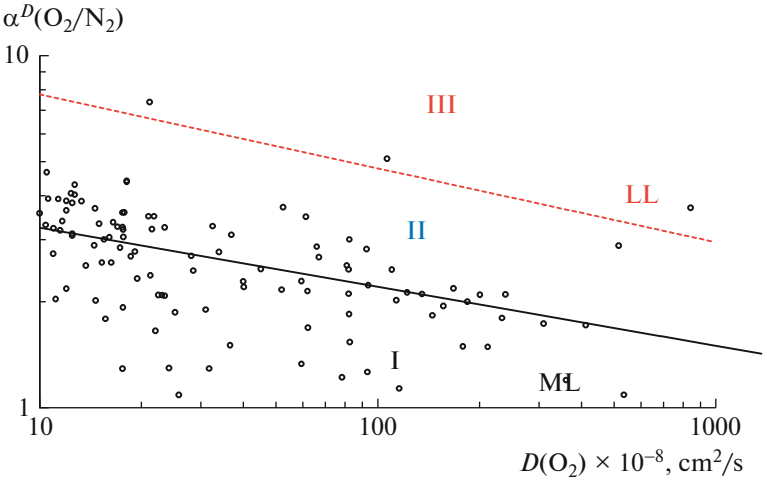

Fig. 2. Fragmented permeability coefficient-permselectivity diagram for the gas pair oxygen/nitrogen [12]. See text for explanations.

with the introduction of bulky substituents conventional for the chemistry of polyheteroarylenes [17, 18], became decisive for the synthesis of new polyheteroarylenes. The position of the Robeson "upper bound" after 2015 is defined by exactly this group of polymers [10, 11].

Figure 1 shows how the "upper bound" shifts to the region of higher permeability and selectivity of a polymeric material in the course of time; a similar dependence is available in [12].

For any polymer, the experimentally measured values of P and α make it possible to estimate using Eq. (4) and Table 1 in what region of the diagram this polymer will be located and what will be the potential of the used design element of the chemical structure of its monomer unit. For example, if a polymer is located in region I for "common" polymers, it does not hold great promise for membrane gas separation (Fig. 1). Polymers situated in the region of the "upper bound" UB1991 are few in number and may be considered fairly promising. Even a smaller number of promising polymers are located in region II and especially near the "upper bound" UB2008. Finally, rare polymers belonging to region III and, especially to the region near the "upper bound" UB2015, are extremely promising. Very few unique polymers belong to region IV [10, 11]. This review covers design elements of the chemical structure of polymers which determine their position on the Robeson diagrams for oxygen/nitrogen and carbon dioxide/methane gas pairs.

According to [8, 9], the position of a polymer on a diagram is primarily determined by diffusivity selectivity α^D. The authors of [12] constructed D–α^D diagrams (Fig. 2) for various gas pairs, and it was shown that the polymers determining empirical "upper bounds" on the permeability–permselectivity diagram usually define orientation of the cloud of data points on the D–α^D diagrams. An example of such a

Table 2. Gas-separation characteristics and positions on the Robeson diagrams and D–α^D diagrams for the polymers of intrinsic microporosity

	P, Barrer		α		$D \times 10^8$, cm^2/s		α^D		Region on the Robeson diagram*		Region on the D–α^D diagram *		References
Polymer	O_2	CO_2	O_2/N_2	CO_2/CH_4	O_2	CO_2	O_2/N_2	CO_2/CH_4	O_2/N_2	CO_2/CH_4	O_2/N_2	CO_2/CH_4	
PIM-1	370–1600	2300–11500	2.6–4.0	9–18	81–270	26–120	2.8–3.7	3.0–3.8	II – UB2008	UB2008 – IV	II	I – ML	[14, 28–31]
PIM-7	190	1100	4.5	6.8	62	21	3.9	4.1	UB2008	UB2008	II	ML	[14]
Cardo-PIM-1	59	430	4.5	20	23	8	3.8	4	II	UB2008	II	I	[32]
SBF-PIM	2640	13900	3.4	13	420	180	3.3	4.3	III	III	LL	LL	[33]
PIM-EA-TB	2150	7140	4.1	10	320	87	3.2	2.4	III	UB2008	LL	I	[34]
PIM-SBI-TB	720	2900	3.1	6.4	201	74	2.7	2.4	II	UB1991	II	I	[34]
PIM-Trip-TB	2720	9700	4.3	11	460	110	3.4	2.3	UB2015	UB2008	LL	I	[35]
PIM-BTrip-TB	3290	13200	3.6	9.2	350	99	5.0	3.5	III	UB2008	III	ML	[36]
TB-Ad-Me	40.2	201	3.6	11	27	10	3.0	3.8	I	I	ML	I	[37]
TPIM-1	370–200	1550	4–6.8	31–32	270–610	24	3.6–6.6	8.4	III – UB2015	III	III – LL	II	[30, 38]
TPIM-2	100–510	390–430	4.4–5.6	21–24	25– 35	11	4.8– 5.1	9	UB2008	II	II	II	[30, 38]
PIM-TMB-Trip	7470	33300	3.4	9.7	–	–	–	–	III	III	–	–	[30, 39]
PIM-TMB-SBI	3200	17500	3.0	8.3	–	–	–	–	UB2008	UB2008	–	–	[30, 39]
PIM-HPB-2	217	1730	3.3	14	940	46	2.7	3.3	UB1991	II	II	ML	[40]

* Hereinafter abbreviations denoting the region of experimental data points on the Robeson diagrams and D–α^D diagrams correspond to designations on the diagrams whose examples are given in the text.

diagram for the gas pair oxygen/nitrogen is shown in Fig. 2 [12]. In addition, upper bounds (limiting lines, **LLs**) were depicted on the diagrams for the diffusion coefficients [12]. The authors of [12] also indicated the so-called "average lines" or distribution "medians" (medianlines, **MLs**) demonstrating the values of the average diffusion selectivity in relation to the diffusion coefficient of the entire data set for glassy amorphous polymers. Equations for these "medians" (MLs) for both permeability coefficients and diffusion coefficients are similar in form to Eq. (4) and stem from the theory of free volume for polymers [12, 19].

Equations of the fluctuation free volume theory developed for diffusion in liquids are also applicable to nonequilibrium glassy polymers with the "frozen" free volume [19]. In accordance with modern ideas, the structure of glassy amorphous polymers is microheterogeneous [2, 19, 20] and it composed of microvoids ("holes") surrounded by a denser packed polymer matrix ("walls"). The average size of "holes" may be evaluated by independent probe methods [19–23], and the average concentration of "holes" N_h in the polymer may be assumed to be almost constant [19, 21, 22] ($N_h = (4–6) \times 10^{20}$ "holes"/cm^3 [19, 22]). Hence, it follows that the level of P and D values is controlled by packing of the polymer in general, that is, the characteristic size of "holes," and selectivity is determined by the average thickness of "walls" [19, 22] and the packing order of chains in "walls" [24]. The value of diffusion selectivity α^D [24] and its deviation from the distribution "median" may serve as a measure of this order [12]. Under first approximation, it may be assumed that for glassy polymers the position of the data point on the diffusion coefficient–diffusion selectivity diagram determines the possible packing order of chains in a polymer. If the data point belongs to the region of the "medianline" (ML), the chain packing is chaotic as in the "conventional" amorphous polymer. If the data point is situated in region II, then the probability of appearance of chain packing order in "walls" becomes higher. If the data point belongs to the upper bound (LL), a high chain packing order in "walls" is very probable. Finally, if the data point is in region I, the chain packing is disordered even compared with the "common" amorphous state. In this review, the possibility of chain packing order is analyzed for highly permeable polyheteroarylenes according to the position of data points on the D–α^D diagram for oxygen/nitrogen and carbon dioxide/methane gas pairs.

DESIGN ELEMENTS OF CHEMICAL STRUCTURE OF HIGHLY PERMEABLE POLYHETEROARYLENES

The main design elements of the chemical structure of thermally stable polyheteroarylenes are kinks in combination with a high rigidity of chains; the introduction of moieties, including spiro moieties, withdrawing the main chain from the planar orientation ("in-plane"); and the introduction of bulky side groups.

Stiff kinks, especially for the polymers of intrinsic microporosity PIMs, commonly lead to the synthesis of rigid-chain ladder or pseudoladder polymers with a low packing density of chains and high fractional free volume and gas permeability [25]. All these polymers are thermally stable, and their glass transition temperature is higher than the decomposition temperature (>350°C). For them the dense packing of macromolecules is not realized in the glassy state, which facilitates formation of nonequilibrium free volume elements (or "holes") of the nanometer size (microporosity). For example, according to positron annihilation, the diameter of holes for PIM-1 is 10–12 Å, whereas for PTMSP it is 12–14 Å [26]. As for most glassy silicon-containing polymers with a high free volume [7], these features of chain packing are responsible for the instability of gas-separation characteristics related to the casting of films from various solvents, the presence of moisture, and the time of aging, which considerably limits their use in practice. These polymers, like silicon-containing polymers with a high free volume [7], demonstrate a marked change in gas-separation characteristics during swelling in alcohols or under physical aging [25]. The introduction of the above-mentioned moieties into polyimides and other polycondensation polymers also promotes an increase in gas permeability but drawbacks related to the instability of properties still persist.

Design elements that do not allow the main chain to assume the planar orientation are often classified with kink moieties. These design elements may be, for example, hexafluoroisopropylidene spacers $-C(CF_3)_2-$, spiro moieties, and other groups hindering the linear or planar orientation of chains. These design elements are united by a common term "in-plane" and are well studied for polyimides [27].

Finally, bulky side groups in the main chain facilitate the restriction of internal rotation and contribute to an increase in the rigidity of chains [17, 18]. These moieties also cause a reduction in packing density and an increase in gas permeability; this effect was also studied in detail for polyimides [17, 18, 27].

All the above-mentioned design elements will be considered below for highly permeable new polymers of intrinsic microposity, polyimides, polyamides, and other polyheteroarylenes. The data detailed in earlier reviews [25, 27] for chemically modified polymers, thermally rearranged polymers, copolymers, and polymer blends are beyond the scope of this paper.

POLYMERS OF INTRINSIC MICROPORISITY

Ladder polymers of intrinsic microporosity with design elements based on stiff chain kinks with both

main chain spirobis(indane) spacer and other kink variants were synthesized [25]. The chemical structure of the polymers of intrinsic microporosity is outlined below.

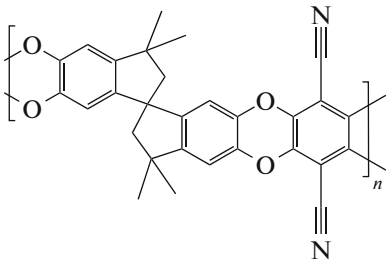

PIM-1

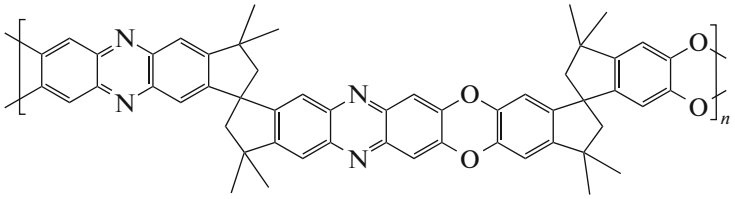

PIM-7

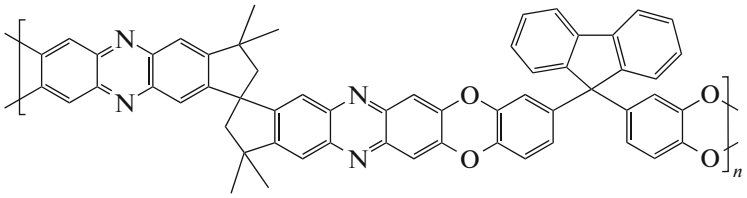

Cardo-PIM-1

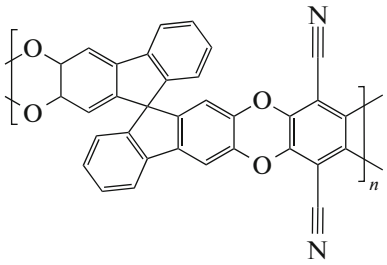

SBF-PIM

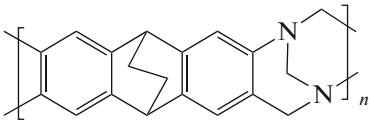

PIM-EA-TB

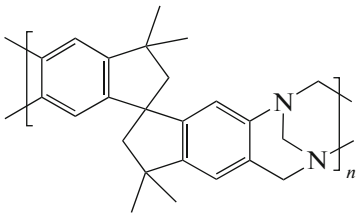

PIM-SBI-TB

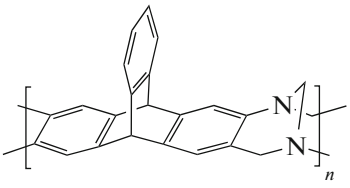

PIM-Trip-TB

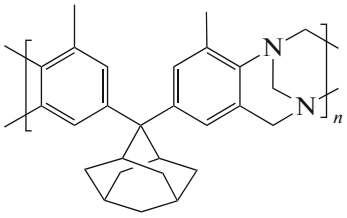

TB-Ad-Me

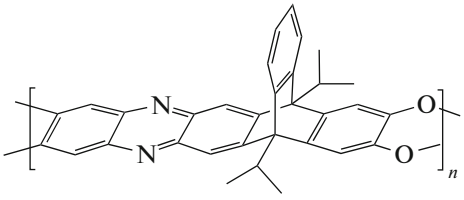

TPIM-1

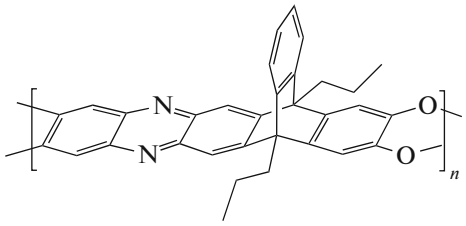

TPIM-2

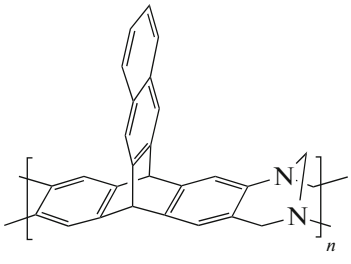

PIM-BTrip-TB

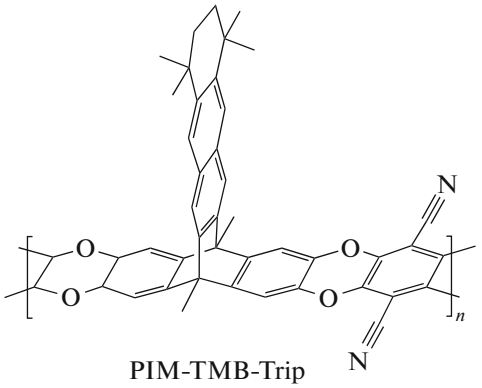

PIM-TMB-Trip

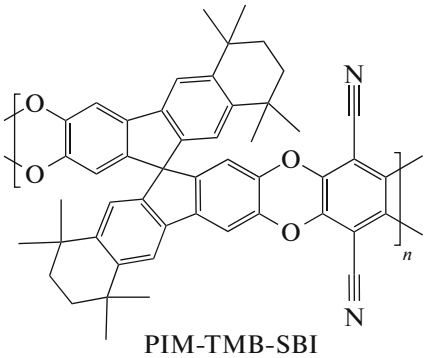

PIM-TMB-SBI

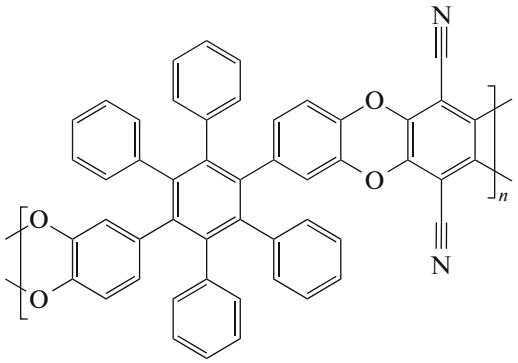

PIM-HPB-2

In the series of polymers with the main chain spirobis(indane) spacer the gas-separation properties of PIM-1 [14, 28–31] and PIM-7 [14] were investigated in length. However, for example, for PIM-1 the value of gas permeability considerably depends on both the synthesis method and subsequent treatment [25, 28, 30, 31]. As a result, there is a marked scatter of the experimental results. Table 2 lists the data only for PIM-1 samples not treated with alcohols. An analysis of diffusion selectivity suggests that for the pair oxygen/nitrogen diffusion characteristics indicate the probable chain packing order while for gases with larger molecules (CO_2/CH_4) this order is absent (Table 2). Probably, this is associated with the specific distribution of packing elements typical of molecular sieves. The introduction of the cardo group into the main chain for Cardo-PIM-1 [32] causes a sharp decrease in permeability, although in its position on the corresponding diagrams this polymer is similar to PIM-1 (Table 2). An increase in the rigidity of the main chain via introduction of the spirobis (fluorene) moiety for SBF-PIM [33], conversely, contributes to rise in permeability and selectivity and moves this polymer to region III on the Robeson diagrams (Table 2). Note that permselectivity grows for the examined gas pairs (LL region in Fig. 2). Apparently, in this case it may be argued that the chain packing order is increased substantially.

Similar rectangular stiff kinks are contained in chain moieties based on ethanoanthracene EA

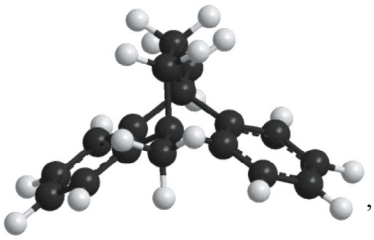

the Tröger base (TB)

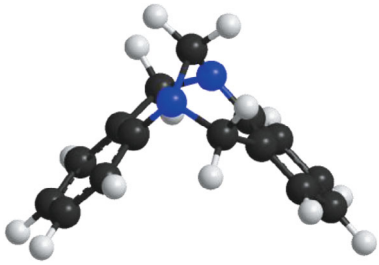

and the triptycene base

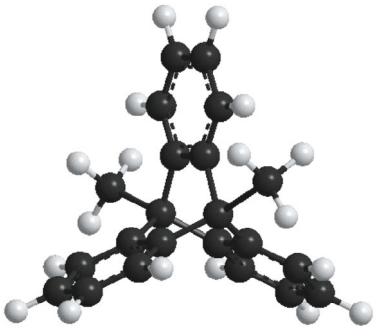

Table 3. Gas-separation characteristics and positions on the Robeson diagrams and D–α^D diagrams for PIM polyimides based on dianhydrides with stiff chain kinks

Polyimide		P, Barrer		α		$D \times 10^8$, cm^2/s		α^D		Region on the Robeson diagram		Region on the on the D–α^D diagram		References
dianhydride	diamine	O_2	CO_2	O_2/N_2	CO_2/CH_4	O_2	CO_2	O_2/N_2	CO_2/CH_4	O_2/N_2	CO_2/CH_4	O_2/N_2	CO_2/CH_4	
SBI-1	TeMPD	150	1100	3.2	14	56	17	2.8	2.4	I(91)	UB1991	ML	I	[41, 42]
SBI-1	4APF	85	520	3.7	19	32	12	3.2	4	I(91)	UB1991	ML	ML	[41, 42]
SBI-1	DMN	545	3700	3.4	14	130	45	3.2	3.2	II	UB2008	II	ML	[41, 42]
SBI-2	TeMPD	640	3200	3.1	9.8	160	64	2.9	2.9	II	II	II	ML	[43]
SBI-2	DMN	710	4100	3.1	12	190	86	3.0	3.4	II	II	II	ML	[43]
EA	DMN	1380	2350–2390	3.7	23–25	270	95	3.2	3.4	III – UB2015	III	II	ML	[46]
KAUST	TeMPD	630–830	7140	4.8–5.9	10	160–230	46–72	4.3–5.1	4.8–7.5	III	UB2008	LL–III	II–LL	[30, 47]
KAUST	TMBZ	490–580	2100	4.4–5.0	21	140–180	49	4.5–4.8	6.2	III	UB2008	LL	II	[30, 47]
KAUST	4APF	370	1540	3.1	20	–	61	–	7.3	UB1991	UB2008	–	LL	[48]
KAUST	DMN	860	–	3.6		180	–	3.4	–	UB2008	–	II	–	[30]
KAUST	mPDA	65	350	4.5	6.3	19	7.0	5.0	32	II	II	II	ML	[49]
KAUST	mPDA(OH)$_2$	32	215	5.5	8.7	8.2	3.8	5.9	46	II	UB2008	II	II	[49]
SBI-2	SBI	210	1500	3.2	12	–	–	–	–	UB1991	UB1991	–	–	[43]
SBI-1	SBF	110	610	3.9	15	–	20	–	4.1	UB1991	UB1991	–	ML	[50]
SBI-1	SBF-Br2	240	1340	3.5	13	–	30	–	3.3	UB1991	UB1991	–	I	[50]
SBI-2	TB	1130	5140	3.0	8.7	210	67	3.1	2.5	II	II	II	I	[51]
SBF	TB	940	4470	3.6	12	190	58	3.4	3.3	UB2008	II	II	ML	[51]
SBI-1	TB1	190	895	5.4	20	94	14	4.6	2.6	III	II	LL	I	[52]
SBI-1	TB2	240	1210	4.9	19	110	23	4.2	3.1	UB2008	II	LL	I	[52]

Upon introduction of EA and TB moieties into the main chain highly permeable polymers PIM-EA-TB and PIM-SBI-TB were synthesized [34]; the authors termed them organic molecular sieves. On the Robeson diagrams PIM-EA-TB is located in region III above or near the 2008 "upper bound." According to diffusion selectivity for O_2/N_2, this polymer demonstrates a high packing order while for gases with large diameter molecules (CO_2/CH_4) the packing order is low (Table 2). Indeed, this evidence suggests that it can be placed in the category of organic molecular sieves. At the same time, for PIM-SBI-TB decrease in both gas-separation parameters on the Robeson diagrams and packing order derived from the diffusion selectivity is observed (Table 2).

The combination of Tröger bases with the triptycene spacer PIM-Trip-TB [35] and benzotriptycene spacer PIM-BTrip-TB [36] made it possible to synthesize polymers with similar properties. These polymers are also located in region III and on the 2008 Robeson "upper bound" (Table 2). Just this group of polymers served as a basis for constructing new "upper bounds" of 2015 [10, 11]. According to the diffusion selectivity behavior of the mentioned polymers (Table 2), especially of PIM-BTrip-TB (region III), they may be assigned to ordered polymeric molecular sieves. However, the combination of a bulky adamantane group with the Tröger base TB-Ad-Me [36] evidently increases the flexibility of chains and, therefore, decreases the packing order and diffusion selectivity and, accordingly, all gas-separation characteristics (Table 2).

The introduction of triptycene moieties into PIM-like structures allowed the authors of [30, 38] to synthesize highly permeable and highly selective ladder polymers TPIM-1 and TPIM-2, also called polymeric molecular sieves. Packing order in these polymers is confirmed by a high diffusion selectivity (Table 2). On the Robeson diagram for O_2/N_2 TPIM-1 with the isopropyl substituent determines the 2015 "upper bound," and its isomer TPIM-2 with the *n*-propyl substituent is located on the 2008 "upper bound" (Table 2). Similar properties [30, 39] are inherent of PIM-1 analogs containing tetramethylhexyl substituents in benzotriptycene PIM-TMB-Trip and cardo PIM-TMB-SBI moieties. In the level of gas permeability these polymers rank much above TPIM (Table 2).

Another design element with stiff kinks for PIM-like structures was the introduction of substituted hexaphenylbenzene moieties [40]. However, polymers of the PIM HPB series noticeably rank below triptycene polymers in gas-separation characteristics and diffusion selectivity (Table 2).

For the overwhelming number of polymers of intrinsic microporosity permeability increases upon alcohol treatment; therefore, gas-transport and gas-separation parameters are often reported only for films treated with alcohols [30, 34, 35, 39]. Particular attention is given to the processes of physical aging, which are accompanied by a decrease in permeability and an increase in selectivity. Therefore, Table 2 lists only the characteristic values of gas-separation parameters for the given polymers without regard to the prehistory and film treatment methods. Additional information is available in the review [25] and original papers.

PIM POLYIMIDES

A drawback of polymers of intrinsic microporosity, along with instable gas-transport characteristics, is a low mechanical strength of films. It was therefore quite natural to use design elements with main chain stiff kinks for the synthesis of new polyimides possessing good film-forming properties. By analogy, this group of polymers was referred to as PIM polyimides. In the synthesis of new dianhydrides and diamines such main chain design elements as spirobis(indane) and spirobis(fluorene) moieties, ethanoanthracene, triptycene, and benzotriptycene spacers, and Tröger base groups, were used. New dianhydrides and diamines with stiff kink elements are depicted below.

Dianhydrides:

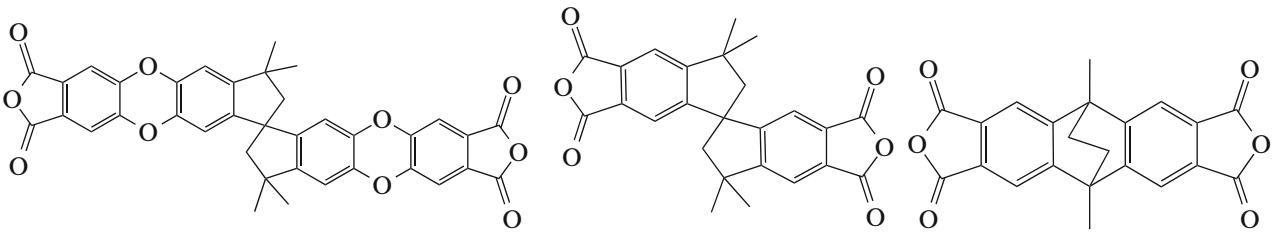

SBI-1 SBI-2 EA

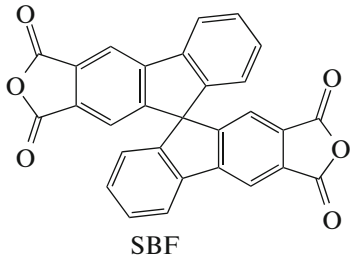
SBF

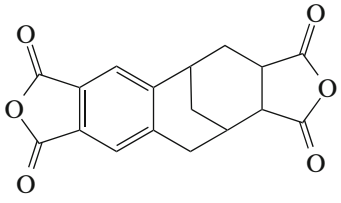
pseudo-TB

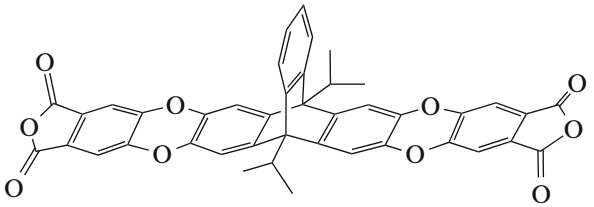
KAUST

Diamines:

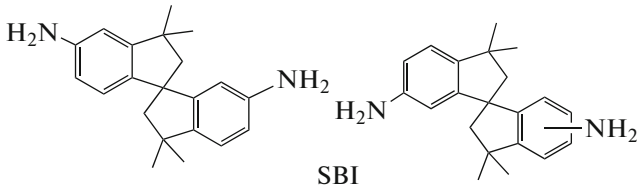
SBI

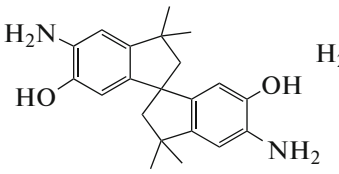
SBI-OH

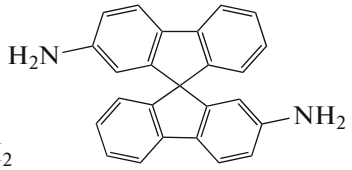
SBF

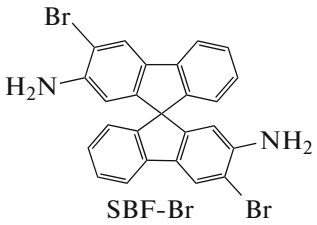
SBF-Br

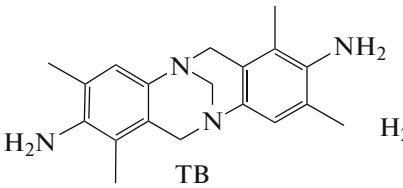
TB

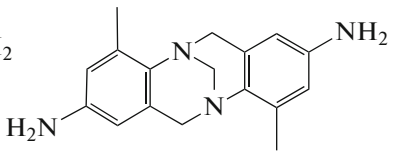
TB1

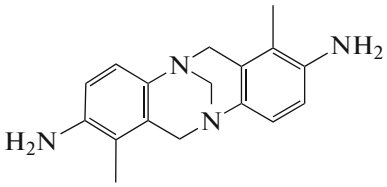
TB2

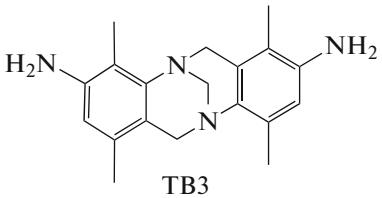
TB3

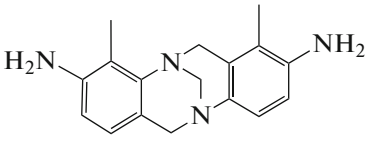
TB4

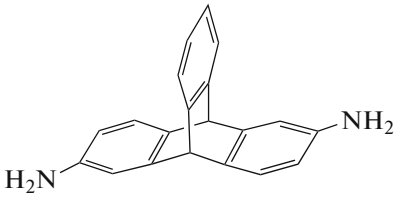
Trip

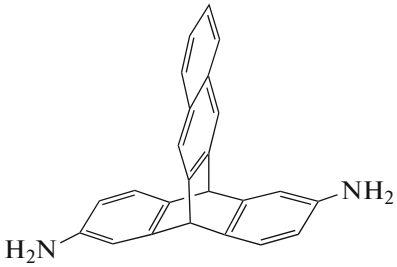
BTrip

The second components in the synthesis of PIM polyimides were well-known dianhydrides

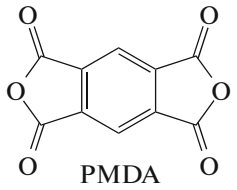

PMDA

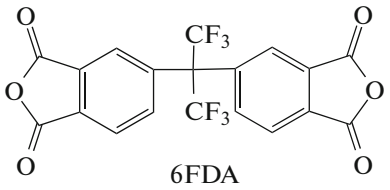

6FDA

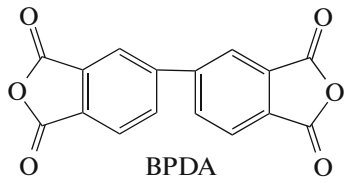

BPDA

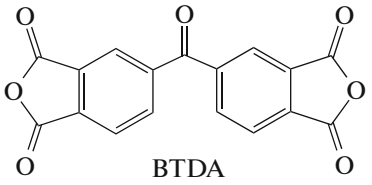

BTDA

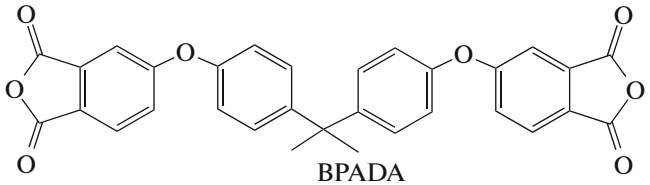

BPADA

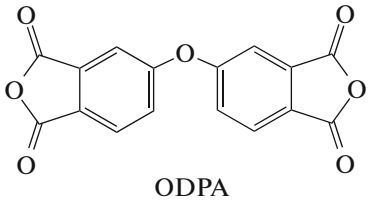

ODPA

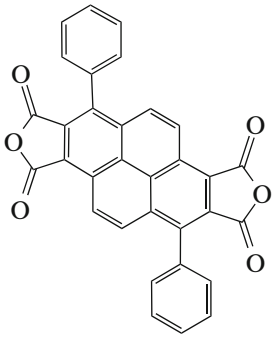

DPPTD

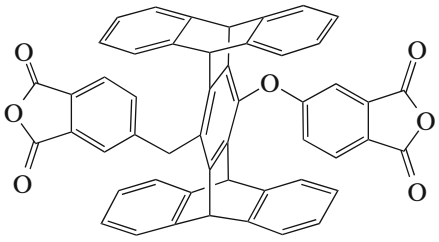

PPDAn

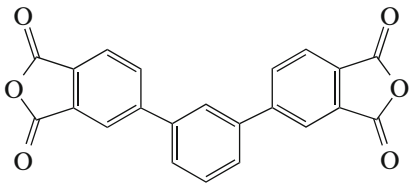

TPDA

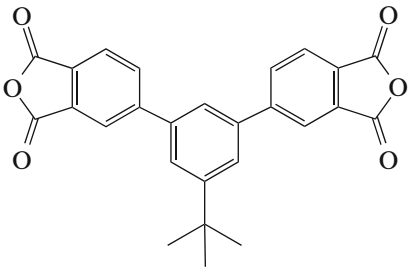

BTPDA

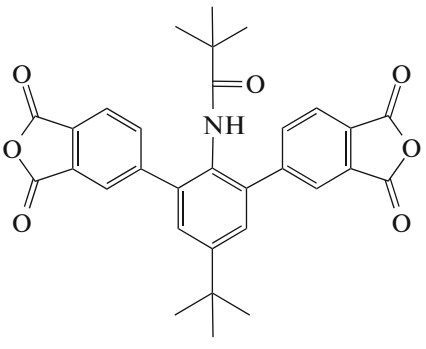

PBTPDA

and diamines

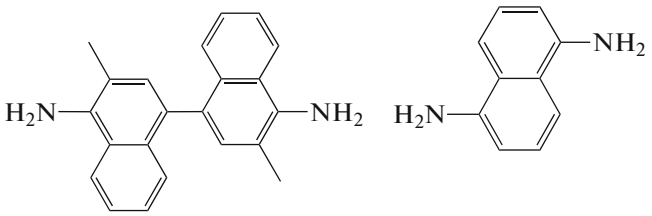

DMN NDA

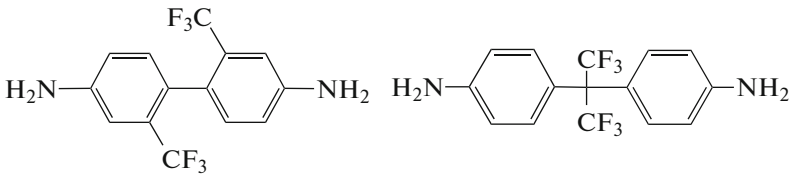

TFDB 4APF

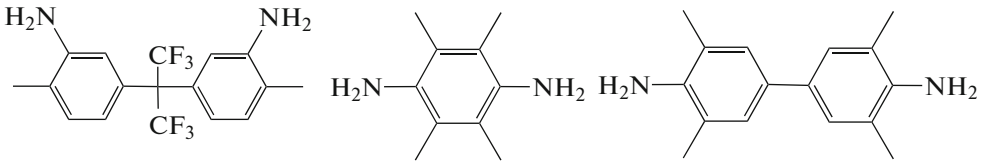

DM4APF TeMPD TMBZ

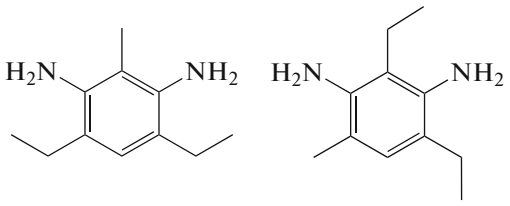

DETDA

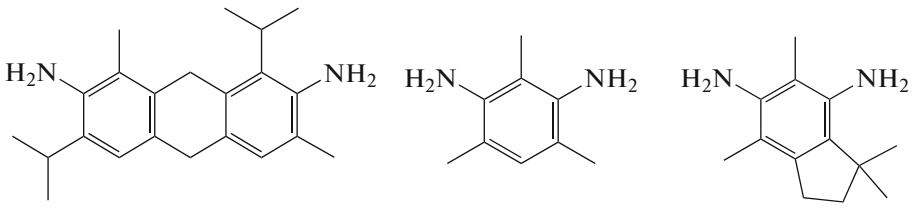

IMM TMPD TMID

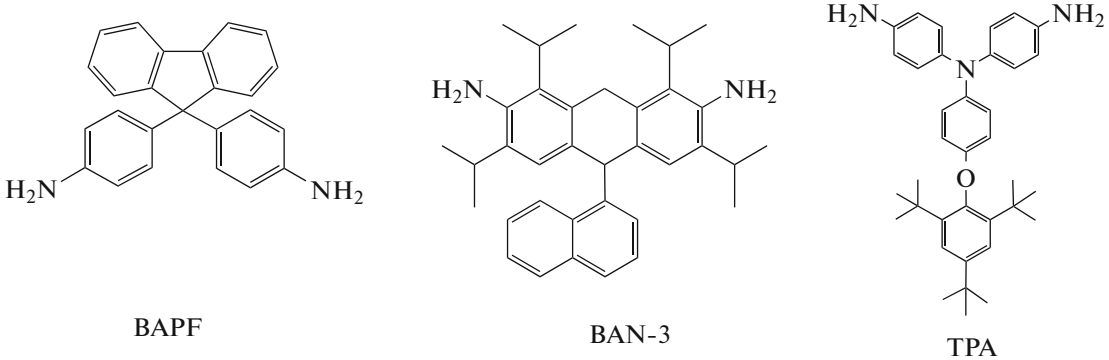

BAPF BAN-3 TPA

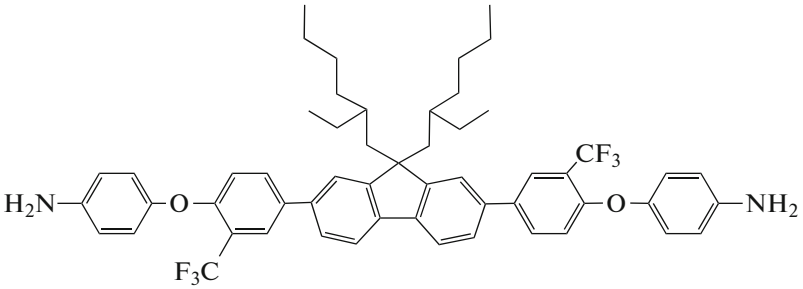

EATPF

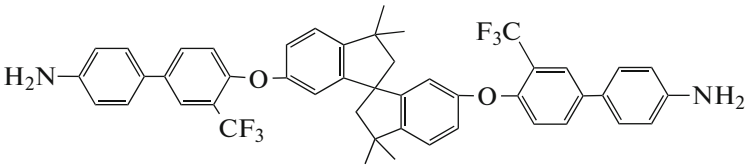

SPBDA

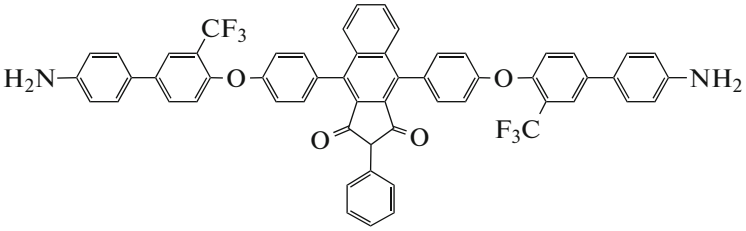

BIDA

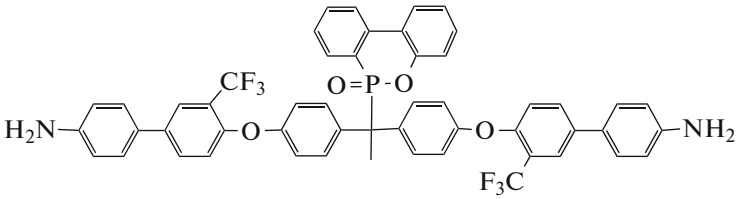

PPADA

The first studied group of highly permeable PIM polyimides ($P(O_2)$ = 64–550 Barrer) includes PIs based on spirobis(indane dianhydride) SBI-1 and diamines DMN, NDA, TFDB, 4APF, DM4APF, and TeMPD [41, 42]. Such a high permeability is very unusual for PIs [6]. On Robeson diagrams these polymers are located near the 1991 "upper bound" [42], and on the CO_2/CH_4 diagram only some of them (DMN, NDA) attain region II, approaching the 2008 "upper bound." The diffusion selectivity for these PIs is low (Table 3). Nevertheless, for PI with diamine DMN the diffusion selectivity reaches region II for the gas pair O_2/N_2, like for PIM-1. Similar gas-separation and diffusion characteristics of this PI and PIM-1 (Table 2) indicate that the chain packing order in the polymers is similar.

PIs based on spirobis(indane) dianhydride SBI-2 and diamines DMN and TeMPD are also highly permeable ($P(O_2)$ = 640–710 Barrer) [43]. On the Robeson diagrams they are located in region II (Table 3), and their diffusion characteristics are similar to those of PIM-1 (Table 2).

PIs derived from diamine DMN and dianhydrides SBF and bicyclooctene pseudo-TB also possess very high gas permeability. For example, for SBF-DMN $P(O_2)$ is 850–1190 Barrer [44] and for pseudo-TB-DMN $P(O_2)$ is 320–850 Barrer [45]. On the Robeson diagrams both polymers are located on the 2008 "upper bounds."

PI synthesized from ethanoanthracene dianhydride EA and diamine DMN [46] is characterized by even higher gas permeability, and $P(O_2)$ attains values

record among PI values, about 1400 Barrer. On the Robeson diagram for O_2/N_2 this polymer forms the 2015 "upper bound," and on the Robeson diagram for CO_2/CH_4 it reaches region III (Table 3). In diffusion characteristics this PI is also similar to PIM-1 (Table 2).

In terms of diffusion characteristics (Table 3) the most ordered packing is exhibited by highly permeable PIs based on triptycene dianhydride KAUST [30, 47–49] and diamines TeMPD and TMBZ [30, 47], 4APF, [48] DMN [30], and mPDA and $mPDA(OH)_2$ [49]. Regardless of diamine on D–α^D diagrams for oxygen/nitrogen and carbon dioxide/methane gas pairs they form the LL upper bound (Table 3), and in the case of KAUST-TeMPD they go beyond its limits to region III. On the Robeson diagrams these PIs are located near the 2008 "upper bounds," and in the case of KAUST-TeMPD and KAUST-TMBZ they are located in region III, although in permeability they rank below EA-DMN. According to these data, these PIs may be classified with ordered polymeric molecular sieves, much more ordered than the majority of polymers of intrinsic microporosity.

The introduction of stiff kink elements simultaneously into dianhydride and diamine moieties also leads to the synthesis of highly permeable PIs; however, the synergistic effect is absent. For example, already the study of PI derived from dianhydride SBI-2 and diamine SBI [43] showed that, as opposed to PIs synthesized using diamines DMN and TeMPD, this PI is both less permeable ($P(O_2) = 210$ Barrer) and less selective: on the Robeson diagrams it is located on the 1991 "upper bound" (Table 3).

The combination of dianhydride SBI-1 with diamine SBF and SBF-Br also resulted in the synthesis of highly permeable PIs ($P(O_2) = 110$–240 Barrer) [50], which are located on the Robeson 1991 "upper bound" (Table 3). According to diffusion selectivity, these polymers demonstrate no order (Table 3).

It was found that the coupling of stiff kink dianhydrides and Tröger base diamine moieties is more effective. For example, the permeability of PI based on dianhydride SBI-2 and diamine TB is very high for polyimides ($P(O_2) = 1130$ Barrer) [51] and on the Robeson diagrams it is located in region II above the 1991 "upper bound" (Table 3). According to the corresponding diffusion selectivity diagram for O_2/N_2, this PI is located in region II. PI based on dianhydride SBF and diamine TB is more selective but less permeable ($P(O_2) = 940$ Barrer) [51]. On the Robeson diagram for O_2/N_2 it is located on the 2008 "upper bound," and, in terms of diffusion selectivity, it also falls in region II (Table 3). PIs based on dianhydride SBI-1 and isomeric diamines TB1 and TB2 are less permeable ($P(O_2) = 190$–240 Barrer) [52] but much more selective. On the Robeson diagram for O_2/N_2 these polymers are now above the 2008 "upper bound" (Table 3), but on the corresponding diffusion selectivity diagram they form the LL upper bound (Table 3). At the same time, for the gas pair CO_2/CH_4 they are less selective, which in general is inherent of polymers of intrinsic microporosity.

As for conventional PIs, the effects of introducing stiff kink elements only into diamine moieties are much less pronounced compared with the introduction of these elements into main chain dianhydride moieties.

For example, only for diamine TB and dianhydride PMDA a high permeability, at a level of stiff kink dianhydrides ($P(O_2) = 1080$ Barrer), is observed [51]. Note that on the Robeson diagrams PI PMDA-TB is located on the 2008 "upper bound" and, likewise PIs based on dianhydrides SBI-2 and SBF, forms the LL upper bound on the corresponding O_2/N_2 diffusion selectivity diagram (Table 4), being less selective for the gas pair CO_2/CH_4. Even for polyimide 6FDA-TB both permeability and selectivity decrease considerably [51], which is reflected on the positions of this PI on the corresponding diagrams (Table 4). For isomeric diamines TB1 and TB2 and dianhydride 6FDA [53] permeability decreases by more than six times compared with analogs based on dianhydride SBI-1 (Tables 3, 4). Although in position on the Robeson diagrams these polymers still occur near "upper bounds," in diffusion selectivity they sharply rank below their analogs (Table 4). For PIs based on the same diamines and dianhydride ODPA [53] reduction in permeability and selectivity is so high that these polymers cease to be highly permeable and on the Robeson diagrams they are located below the 1991 "upper bound" [53].

PIs based on dianhydride 6FDA and diamines TB3 ($T_g = 425$°C) [54] and TB4 ($T_g = 395$°C) [55] demonstrate low permeability (Table 4). On the Robeson diagrams they are near the 1991 "upper bound," although in terms of diffusion characteristics they are located in region II on the corresponding diagram for O_2/N_2 (Table 4). At the same time, polyimides BTDA-TB3 ($T_g = 438$°C) [54], BTDA-TB4 ($T_g = 419$°C), and ODPA-TB4 ($T_g = 428$°C) [55], as in the previous case, cease to be highly permeable and selective [54, 55].

For PIs based on dianhydrides 6FDA and PMDA and diamine SBF permeability, selectivity, and diffusion characteristics also decrease sharply compared with the analog based on dianhydride SBI-1 [50] (Tables 3, 4). For the same dianhydrides and diamine SBF-Br differences are not so distinct but the tendency is preserved (Table 4). Note that there are almost no differences in the properties of PIs based on dianhydrides 6FDA and PMDA, in contrast to PI based on diamine TB [51]. Similar dependences are also typical of PIs based on dianhydrides 6FDA and PMDA and diamine SBI-OH [56, 57] (Table 4). PIs prepared using dianhydrides BPDAs and BPADA and diamine SBI-OH [57] are medium-permeable, and on

Table 4. Gas-separation characteristics and positions on the Robeson diagrams and D–α^D diagrams for PIM polyimides based on diamines with stiff chain kinks

Polyimide		P, Barrer		α		$D \times 10^8$, cm^2/s		α^D		Region on the Robeson diagram		Region on the D–α^D diagram		References
dianhydride	diamine	O_2	CO_2	O_2/N_2	CO_2/CH_4	O_2	CO_2	O_2/N_2	CO_2/CH_4	O_2/N_2	CO_2/CH_4	O_2/N_2	CO_2/CH_4	
PMDA	TB	1080	4460	3.7	11	195	41	4.0	2.7	UB2008	II	LL	I	[51]
6FDA	TB	410	1700	3.1	14	100	26	2.9	3.0	UB1991	II	II	I	[51]
6FDA	TB1	28	155	4.3	47	–	3.4	–	4.2	UB1991	II	–	I	[53]
6FDA	TB2	47	285	3.9	36	–	5.3	–	4.8	I(91)	II	–	ML	[53]
6FDA	TB3	120	460	3.8	17	38	13	3.6	4.1	UB1991	UB1991	II	ML	[54]
6FDA	TB4	42	220	4.4	33	18	6.1	4.1	6.4	UB1991	II	II	ML	[55]
6FDA	SBF	35	180	4.5	28	–	7.2	–	6.0	UB1991	UB1991	–	ML	[50]
PMDA	SBF	36	200	4.2	22	–	6.0	–	5.1	UB1991	UB1991	–	ML	[50]
6FDA	SBF-Br	110	580	4.0	23	–	17	–	5.3	UB1991	II	–	ML	[50]
PMDA	SBF-Br	120	690	3.8	19	–	17	–	5.0	UB1991	II	–	ML	[50]
6FDA	SBI-OH	22–45	100–260	4.2	24–29	11	6.3–8.0	3.0	4.9–7.9	I-UB1991	UB1991-II	ML	ML-II	[56, 57]
PMDA	SBI-OH	31–40	200–240	4.0–4.4	17–26	–	9.9	–	4.9	I-UB1991	UB1991	–	ML	[56, 57]
6FDA	Trip	25–39	120–190	4.8–5.4	30–38	15–23	8.2–13	3.8–4.2	8.7–11	UB1991	II	II	II	[58, 59]
6FDA	BTrip	43	210	4.8	30	24	14	3.8	8.9	UB1991	II	II	II	[59]
6FDA	TeMPD-PPDAn-TeMPD	–	810	–	27	–	35	–	4.7	–	UB2008	–	II	[60]

Table 5. Gas-separation characteristics and positions on the Robeson diagrams and D–α^D diagrams for polyimides based on diamines with main chain bends

Polyimide		T_g, °C	P, Barrer		α		$D \times 10^8$, cm^2/s		α^D		Region on the Robeson diagram		Region on the D–α^D diagram		References
dianhydride	diamine		O_2	CO_2	O_2/N_2	CO_2/CH_4	O_2	CO_2	O_2/N_2	CO_2/CH_4	O_2/N_2	CO_2/CH_4	O_2/N_2	CO_2/CH_4	
DPPTD	4APF	525	44	260	4.0	20	18	10	3.6	5.2	I(91)	I(91)	II	ML	[64]
DPPTD	IMM	490	75	390	3.9	16	29	14	3.5	4.5	I(91)	I(91)	II	ML	[64]
DPPTD	TMPD	560	280	1600	3.8	15	53	37	3.5	5.5	II	II	II	II	[64]
6FDA	DETDA	368	76	350	3.5	19	–	–	–	–	I(91)	I(91)	–	–	[65]
6FDA	DETDA	400	82	450	3.4	20	36	12	2.8	3.4	I(91)	UB1991	ML	I	[66]
BPDA	DETDA	>450	28	200	3.9	19	14	4.6	3.2	3.3	I(91)	I(91)	ML	I	[66]
PMDA	TBAPB	329	23	140	4.0	18	19	11	2.8	4.7	I	I	ML	ML	[67]
PMDA	TMPD	565	89	530	4.0	24	23	9.2	3.8	4.4	UB1991	II	II	ML	[68]
PMDA	TMID	525	230	1190	4.0	16	51	21	3.3	3.8	II	II	II	ML	[68]
TDPA	TMPD	414	27	140	4.5	20	11	5	3.1	5.6	I	I	ML	ML	[69]
BTPDA	TMPD	367	110	465	3.7	12	30	15	2.6	3.5	I(91)	I	ML	I	[69]
PBTPDA	TMPD	420	35	210	4.0	18	16	8.6	2.8	3.7	I	I	ML	I	[69]
ODPA	BAN-3	–	47	230	3.4	16	2.8	0.85	4.8	3.4	I	I	ML	I	[70]
BPDA	BAN-3	–	81	390	5.0	15	3.7	1.5	4.1	3.6	II	I	ML	I	[70]
6FDA	BAN-3	–	100	845	1.9	15	1.7	2.7	1.5	2.6	I	UB1991	I	I	[70]
6FDA	SPBDA	269	36	53	11	44	23	6.3	4.6	1.6	IV	UB1991	II	I	[73]
6FDA	BIDA	315	25	71	6.0	36	14	3.3	4.2	2.2	II	UB1991	II	I	[74]
6FDA	PPADA	261	64	175	7.1	51	22	20	3.3	6.5	III	UB2008	ML	II	[75]
BPADA	PPADA	235	57	110	6.1	45	21	17	3.6	6.9	UB2008	II	II	II	[75]
ODPA	PPADA	251	40	97	6.3	51	16	16	3.4	7.0	UB2008	UB2008	ML	II	[75]
BTDA	PPADA	258	34	94	6.4	49	16	15	3.1	7.0	UB2008	II	ML	II	[75]
BPDA	TPA	230	27	76	7.2	48	–	–	–	–	UB2008	II	–	–	[76]
6FDA	TPA	260	21	65	7.3	48	–	–	–	–	UB2008	II	–	–	[76]
ODPA	TPA	270	40	100	7.8	51	–	–	–	–	UB2008	II	–	–	[76]

the Robeson diagrams they are located below the 1991 "upper bound."

As in the case of PIs based on triptycene dianhydrides, PIs derived from triptycene Trip [58, 59] and benzotriptycene BTrip [59] diamines and dianhydride 6FDA demonstrate a high diffusion selectivity (Table 4); at the same time, their gas permeability is much lower compared with PI based on dianhydride KAUST (Table 3). And only PI based on dianhydride 6FDA and complex diamine with the pentitriptycene moiety TeMPD-PPDAn-TeMPD ($T_g > 400$°C), which can be regarded as a regular copolyamide of diamine TeMPD and dianhydrides 6FDA and PPDAn, owing to a high CO_2 permeability [60], is located on the Robeson 2008 "upper bound" for the gas pair CO_2/CH_4 and is located in region II on the corresponding diffusion selectivity diagram (Table 4).

POLYHETEROARYLENES WITH MAIN CHAIN BENDS

Design elements, such as "in-plane" or side chain bulky substituents, have a similar effect on the properties of polymers. Owing to the limited internal rotation these design elements hinder the linear or planar orientation of chains; as a result, packing density decreases and gas permeability increases. As a rule, in these polymers extended linear or planar moieties alternate with sharp chain bends. These design elements are best studied for polyimides [17, 18, 27], and in the present review they are united by a common term "with main chain bends."

Examples of such polymers are polypyrrolones and poly(pyrrolone imides) [61–63], which form the "upper bound" on the 2008 Robeson diagram [6, 9] or are located on the 1991 "upper bound" [6, 63]. Note that their high selectivity is determined by the selectivity of diffusion and is explained by the specific features of packing order; therefore, the authors term them "pseudomolecular sieves" [63]. PIs based on dianhydride DPPTD [64] have an extended planar structure similar to that of polypyrrolones. Accordingly, PIs derived from dianhydride DPPTD and diamines with main chain bends, such as 6F, IMM, and TMPD ("in-plane"), are characterized by a fairly high permeability (Table 5). Even though on the Robeson diagrams these polymers are located near the 1991 "upper bound," their packing order (diffusion selectivity) is very high (region II), especially for diamine TMPD. The structure of diamine DETDA is similar to that of diamine TMPD. PI synthesized suing diamine DETDA and dianhydride 6FDA features high permeability [65]. On the Robeson diagrams this polymer is situated near the 1991 "upper bounds." PIs based on a mixture of isomeric diamines DETDA and dianhydrides 6FDA and BPDA are also highly permeable [66]. On the Robeson diagrams they are also located near the 1991 "upper bounds" but in terms of diffusion selectivity they do not manifest packing order. PIs based on this diamine but more flexible dianhydrides BTDA, BPADA, and ODPA are not highly permeable and selective [66]. The same behavior is exhibited by PI based on diamine TBAPB [67]. At the same time, PIs synthesized using PMDA and diamines TMPD and TMID are highly permeable (Table 5), especially PI PMDA–TMID [68]. Note that, according to diffusion selectivity for O_2/N_2, both PIs exhibit a fairly high packing order (Table 5).

PIs based on diamine TMPD and dianhydrides TPDA, BTPDA, and PBTPDA with "in-plane" main chain bends and bulky substituents [69] also belong to highly permeable PIs; however, on the Robeson diagrams they do not attain the 1991 "upper bound" and, according to diffusion selectivity, do not manifest the signs of packing order (Table 5).

Similar diffusion selectivity trends are observed for highly permeable PIs based on dianhydrides ODPA, BPDA, and 6FDA with diamine BAN-3 with bulky

Table 6. Gas-separation characteristics and position on the Robeson diagrams and D–α^D plots for polyheteroarylenes with main chain bends

Polymer	T_g, °C	P, Barrer		α		$D \times 10^8$, cm^2/s		α^D		Region on the Robeson diagram		Region on the D–α^D diagram		References
		O_2	CO_2	O_2/N_2	CO_2/CH_4	O_2	CO_2	O_2/N_2	CO_2/CH_4	O_2/N_2	CO_2/CH_4	O_2/N_2	CO_2/CH_4	
POXINAR 2bF	>500	49	280	4.4	21	–	–	–	–	I(91)	UB1991	–	–	[71]
PA 6F2tBu	284	44	170	7.3	24	42	33	2.6	3.7	III	I(91)	ML	ML	[78]
PA 12F2tBu	276	40	160	7.7	31	30	21	2.9	3.5	III	UB1991	ML	I	[78]
PA 6F2tBu	275	20	80	7.4	27	15	9.3	2.6	2.6	UB2008	I	ML	I	[78]
PA 4tBu	263	20	86	8.1	30	9.8	7.8	3.3	2.9	III	I(91)	ML	I	[79]
PA 6F3tBu	271	29	120	9.7	37	14	11	3.9	3.4	UB2015	II	II	I	[79]

substituents and main chain bends [70]. On the Robeson diagram PI derived from dianhydride BPDA is the most selective among them (Table 5).

An interesting example of new polyheteroarylenes with main chain bends is polyisathines carrying various substituents of the POXINAR series [71].

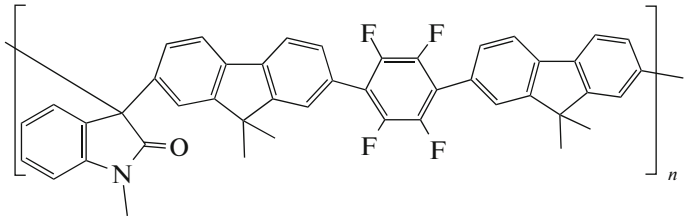

POXINAR 2bF

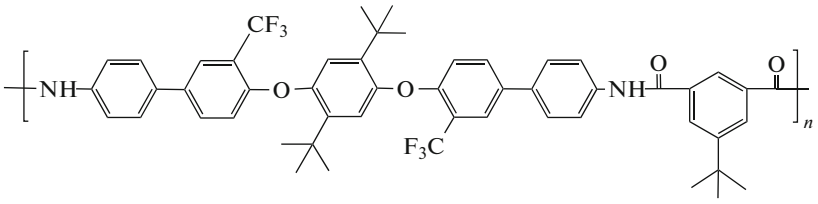

PA 6F2tBu

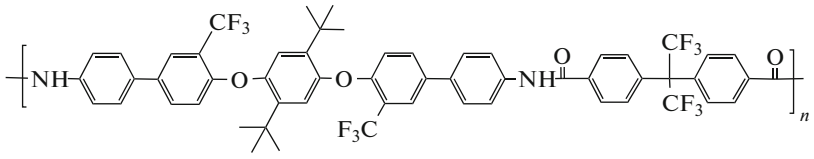

PA 12F2tBu

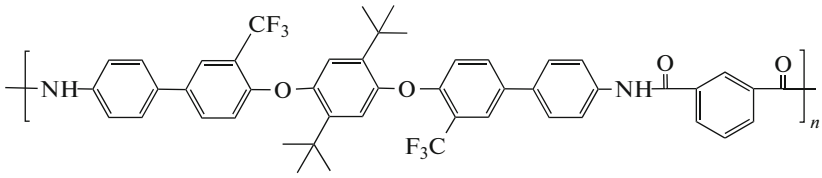

PA 6F2tBu

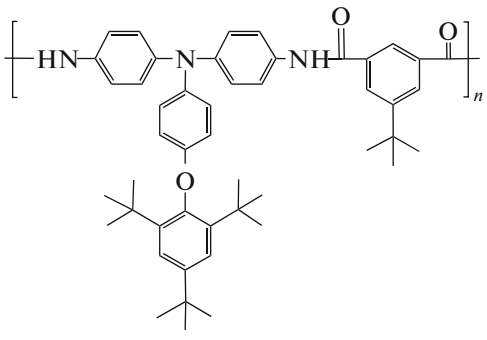

PA 4tBu

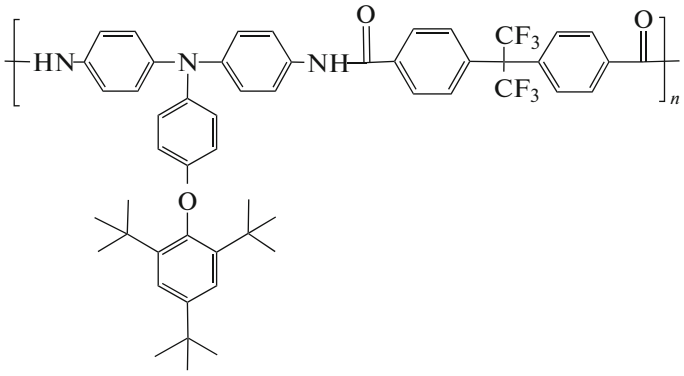

PA 6F3tBu

For these polymers the glass transition temperature is higher than the decomposition temperature (T_g > 500°C), and on the Robeson diagrams they are also located near or on the 1991 "upper bound" [71]. However, the polymer containing a long linear moiety with two fluorene groups is the only highly permeable polymer among polymers of the POXINAR series (Table 6).

At the same time, PI with main chain bends, which is based on spirofluorene diamine BAPF and dianhydride 6FDA (T_g = 383°C) [72], also belongs to highly permeable PIs ($P(O_2)$ = 31 Barrer). On the Robeson diagram for O_2/N_2 it is near the 1991 "upper bound."

Analogous design elements for the synthesis of polyimides, polyimides, and polyesters with main chain bends resulting from the presence of asymmetric centers and bulky side groups are intensively used by S. Banerjee et al. [18, 74]. Many polymers synthesized by this team over the past decade possess high selectivity for the gas pair O_2/N_2 and are located above the 2008 Robeson "upper bound" [18, 74]. For example, PIs based on diamine EATPF and dianhydrides 6FDA, BPADA, ODPA, BTDA, and PMDA are close to highly permeable ($P(O_2)$ = 8.5–17 Barrer) [77]. Their O_2/N_2 selectivity attains 15–20, and on the Robeson diagram for the O_2/N_2 gas pair these polymers are located in region IV above the 2015 "upper bound." Note that the most selective PI derived from dianhydride PMDA ($\alpha(O_2/N_2)$ = 20) is situated in region of the LL upper bound on the diffusion selectivity diagram for O_2/N_2. At the same time, on the Robeson diagrams for the CO_2/CH_4 gas pair these PIs are located in region II or on the 2008 "upper bound" and on the diffusion selectivity diagram CO_2/CH_4 they are located in region I.

PIs synthesized from diamine containing spiro(bis)indane group SPBDA and dianhydrides BPADA, 6FDA, and ODPA are also close to highly permeable ($P(O_2)$ = 9.9–36 Barrer) [73]. The O_2/N_2 selectivity for these polymers is lower than that for PI based on diamine EATPF (9.7–12), and on the Robeson diagram for the O_2/N_2 gas pair they are mostly located in the region of the 2015 "upper bound." In this series of PIs, the most permeable and selective is SPBDA-6FDA, which is situated in region IV above the 2015 "upper bound" of the O_2/N_2 diagram (Table 5).

PIs based on diamine with the lateral planar benzoisoindoledione moiety in the main chain BIDA and dianhydrides BPADA, 6FDA, and BTDA($P(O_2)$ = 7.0–25 Barrer) are also characterized by a high selectivity for the O_2/N_2 gas pair (6.0–8.4) [74]; therefore, on the corresponding Robeson diagram they are located in region II. In terms of diffusion selectivity PI BPADA-BIDA is the most ordered (near the LL upper bound), and the most permeable 6FDA-BIDA is also in region II (Table 5).

An analysis of correlations between the transport characteristics of the mentioned PIs and their free volume values [18, 80] indicates that their high selectivity is largely controlled by a high overall diffusion selectivity.

PIs based on diamine with the asymmetric quaternary carbon atom substituted with the phosphorous-containing group PPADA [75] and dianhydrides 6FDA, BPADA, ODPA, and BTDA are highly permeable and highly selective. On both Robeson diagrams they are located in the region of the 2008 "upper bound" and manifest the signs of order according to the diffusion selectivity diagram. PIs derived from triphenylamine with a bulky side substituent [76] and dianhydrides BPDA, 6FDA, and ODPA also belong to the group of highly permeable and highly selective PIs (Table 5).

Similar design elements were used for the synthesis of highly permeable polyamides ($P(O_2)$ = 11–44 Barrer) [78, 79]. All of them are located on the Robeson diagram for the O_2/N_2 gas pair in the region of the 2008 "upper bound" and in region III, achieving also the 2015 "upper bound" (Table 6). At the same time, as regards CO_2/CH_4 selectivity they rank much below and do not go beyond the 1991 "upper bound" on the corresponding Robeson diagram. In terms of diffusion selectivity the polyamides under consideration do not manifest a considerable packing order (Table 6).

CONCLUSUONS

Thus, the introduction of both bulky side moieties leading to main chain bends due to the hindrance of internal rotation and moieties withdrawing the main chain from the planar orientation ("in-plane") and also causing the appearance of main chain bends, in terms of their effect on chain packing, appears to be similar to the effect of stiff kinks used in designing polymers of intrinsic microporosity and PIM polyimides. These design elements to a different extent contribute to the formation of low-density packing, and, accordingly, high permeability of polymers. Both stiff kinks and regular main chain bends entail formation of ordered chain packing. The higher this order, the higher the diffusion selectivity and the higher, eventually, the selectivity of the material. Owing to these specific features the chain packings of highly permeable polyheteroarylenes considered in this review form the Robeson "upper bounds" and may be characterized as polymeric molecular sieves determining the modern permeability/selectivity trade-off relationship of polymeric materials.

FUNDING

This work was supported by the Russian Science Foundation (project no. 19-19-00614).

REFERENCES

1. R. W. Baker and B. T. Low, Macromolecules **47**, 6999 (2014).
2. *Materials Science of Membranes for Gas and Vapor Separation,* Ed. by Yu. Yampolskii, I. Pinnau, and B. Freeman (Wiley, Chichester, 2006).
3. Y. Yampolskii, Macromolecules **45**, 3298 (2012).
4. R. W. Baker, Ind. Eng. Chem. Res. **41**, 1393 (2002).

5. A. F. Ismail, K. C. Khulbe, and T. Matsuura, *Gas Separation Membranes. Polymeric and Inorganic* (Springer Int. Publ. Switzerland, Heidelberg; New York; Dordrecht; London, 2015).
6. *"Gas Separation Parameters of Glassy Polymers" Database* (Informregistr RF, 1998) [in Russian].
7. *Membrane Materials Science for Gas and Vapor Separation,* Ed. by Y. Yampolskii and E. Finkelshtein (Wiley, Chichester, 2017).
8. L. Robeson, J. Membr. Sci. **62**, 165 (1991).
9. L. Robeson, J. Membr. Sci. **320**, 390 (2008).
10. R. Swaidan, B. Ghanem, and I. Pinnau, ACS Macro Lett. **4**, 947 (2015).
11. B. Comesana-Gandara, J. Chen, C. G. Bezzu, M. Carta, I. Rose, M.-C. Ferrari, E. Esposito, A. Fuoco, J. C. Jansen, and N. B. McKeown, Energy Environ. Sci. **12**, 2733 (2019).
12. A. Alentiev and Yu. Yampolskii, Ind. Eng. Chem. Res. **52**, 8864 (2013).
13. P. M. Budd, B. S. Ghanem, S. Makhseed, N. B. McKeown, K. J. Msayib, and C. E. Tattershall, Chem. Commun. **2004**, 230 (2004).
14. P. M. Budd, K. J. Msayib, C. E. Tattershall, B. S. Ghanem, K. J. Reynolds, N. B. McKeown, and D. Fritsch, J. Membr. Sci. **251**, 263 (2005).
15. I. I. Ponomarev, I. V. Blagodatskikh, A. V. Muranov, Y. A. Volkova, D. Y. Razorenov, I. I. Ponomarev, and K. M. Skupov, Mendeleev Commun. **26**, 362 (2016).
16. M. Heuchel, D. Fritsch, P. M. Budd, N. B. McKeown, and D. Hofmann, J. Membr. Sci. **318**, 84 (2008).
17. I. A. Ronova, A. Yu. Alentiev, and M. Bruma, Polym. Rev. **58**, 376 (2018).
18. B. D. Ghosh, S. Banerjee, A. Alentiev, I. Ronova, and Yu. Yampolskii, ub *Imidic Polymers and Green Polymer Chemistry: New Technology and Developments in Process and Products,* Ed. by A. I. Barzic, N. K. Rawat, and A. K. Haghi (Apple Acad. Press, New York, 2021), Chap. 2.
19. *Nanomaterials: Properties and Perspective Applications,* Ed. by A. Yaroslavtseva (Nauchnyi mir, Moscow, 2014) [in Russian].
20. Yu. Yampol'skii, Russ. Chem. Rev. **76**, 59 (2007).
21. G. Dlubek, J. Pionteck, K. Rätzke, J. Kruse, and F. Faupel, Macromolecules **41**, 6125 (2008).
22. A. Alentiev and Yu. Yampolskii, J. Membr. Sci. **206**, 291 (2002).
23. V. E. Ryzhikh, A. Y. Alent'ev, and Y. P. Yampol'skii, Polym. Sci., Ser. A **55**, 244 (2013).
24. A. Yu. Alentiev, N. A. Belov, S. V. Chirkov, and Yu. P. Yampolskii, J. Membr. Sci. **547**, 99 (2018).
25. Z.-X. Low, P. M. Budd, N. B. McKeown, and D. A. Patterson, Chem. Rev. **118**, 5871 (2018).
26. V. P. Shantarovich, V. G. Bekeshev, I. B. Kevdina, Yu. P. Yampol'skii, M. V. Bermeshev, and N. A. Belov, High Energy Chem. **52**, 275 (2018).
27. H. Sanaeepur, A. E. Amooghin, S. Bandehali, A. Moghadassi, T. Matuura, and B. Van der Bruggen, Prog. Polym. Sci. **91**, 80 (2019).
28. P. M. Budd, N. B. McKeown, B. S. Ghanem, K. J. Msayib, D. Fritsch, L. Starannikova, N. Belov, O. Sanfirova, Y. P. Yampolskii, and V. Shantarovich, J. Membr. Sci. **325**, 851 (2008).
29. C. L. Staiger, S. J. Pas, A. J. Hill, and C. J. Cornelius, Chem. Mater. **20**, 2606 (2015).
30. R. Swaidan, B. Ghanem, E. Litwiller, and I. Pinnau, Macromolecules **48**, 553 (2015).
31. I. I. Ponomarev, D. Y. Razorenov, I. V. Blagodatskikh, A. V. Muranov, L. E. Starannikova, A. Yu. Alent'ev, R. Yu. Nikiforov, and Y. P. Yampol'skii, Polym. Sci., Ser. B **61**, 605 (2019).
32. B. S. Ghanem, N. B. McKeown, P. M. Budd, and D. Fritsch, Macromolecules **41**, 1640 (2008).
33. C. G. Bezzu, M. Carta, A. Tonkins, J. C. Jansen, P. Bernardo, F. Bazzarelli, and N. B. McKeown, Adv. Mater. **24**, 5930 (2012).
34. M. Carta, R. Malpass-Evans, M. Croad, Y. Rogan, J. C. Jansen, P. Bernardo, F. Bazzarelli, and N. B. McKeown, Science **339**, 303 (2013).
35. M. Carta, M. Croad, R. Malpass-Evans, J. C. Jansen, P. Bernardo, G. Clarizia, K. Friess, M. Lanč, and N. B. McKeown, Adv. Mater. **26**, 3526 (2014).
36. I. Rose, M. Carta, R. Malpass-Evans, M. C. Ferrari, P. Bernardo, G. Clarizia, J. C. Jansen, and N. B. McKeown, ACS Macro Lett. **4**, 912 (2015).
37. M. Carta, M. Croad, J. C. Jansen, P. Bernardo, G. Clarizia, and N. B. McKeown, Polym. Chem. **5**, 5255 (2014).
38. B. S. Ghanem, R. Swaidan, X. Ma, E. Litwiller, and I. Pinnau, Adv. Mater. **26**, 6696 (2014).
39. I. Rose, C. G. Bezzu, M. Carta, B. Comesaña-Gándara, E. Lasseuguette, M. C. Ferrari, P. Bernardo, G. Clarizia, A. Fuoco, J. C. Jansen, K. E. Hart, T. P. Liyana-Arachchi, C. M. Colina, and N. B. McKeown, Nat. Mater. **16**, 932 (2017).
40. R. Short, M. Carta, C. G. Bezzu, D. Fritsch, B. M. Kariuki, and N. B. McKeown, Chem. Commun. **47**, 6822 (2011).
41. B. S. Ghanem, N. B. McKeown, P. M. Budd, J. D. Selbie, and D. Fritsch, Adv. Mater. **20**, 2766 (2008).
42. B. S. Ghanem, N. B. McKeown, P. M. Budd, N. M. Al-Harbi, D. Fritsch, K. Heinrich, L. Starannikova, A. Tokarev, and Y. Yampolskii, Macromolecules **42**, 7881 (2009).
43. Y. Rogan, L. Starannikova, V. Ryzhikh, Y. Yampolskii, P. Bernardo, F. Bazzarelli, J. C. Jansen, and N. B. McKeown, Polym. Chem. **4**, 3813 (2013).
44. X. Ma, B. Ghanem, O. Salines, E. Litwiller, and I. Pinnau, ACS Macro Lett. **4**, 231 (2015).
45. X. Ma, M. A. Abdulhamid, and I. Pinnau, Macromolecules **50**, 5850 (2017).
46. Y. Rogan, R. Malpass-Evans, M. Carta, M. Lee, J. C. Jansen, P. Bernardo, G. Clarizia, E. Tocci, K. Friess, M. Lanč, and N. B. McKeown, J. Mater. Chem. A **2**, 4874 (2014).
47. B. S. Ghanem, R. Swaidan, E. Litwiller, and I. Pinnau, Adv. Mater. **26**, 3688 (2014).
48. R. Swaidan, B. Ghanem, M. Al-Saeedi, E. Litwiller, and I. Pinnau, Macromolecules **47**, 7453 (2014).
49. N. Alaslai, B. Ghanem, F. Alghunaimi, and I. Pinnau, Polymer **91**, 128 (2016).

50. X. Ma, O. Salinas, E. Litwiller, and I. Pinnau, Macromolecules **46**, 9618 (2013).
51. M. Lee, C. G. Bezzu, M. Carta, P. Bernardo, G. Clarizia, J. C. Jansen, and N. B. McKeown, Macromolecules **49**, 4147 (2016).
52. Z. Wang, D. Wang, and J. Jin, Macromolecules **47**, 7477 (2014).
53. Z. Wang, D. Wang, F. Zhang, and J. Jin, ACS Macro Lett. **3**, 597 (2014).
54. Y. Zhuang, J. G. Seong, Y. S. Do, H. J. Jo, Z. Cui, J. Lee, Y. M. Lee, and M. D. Guiver, Macromolecules **47**, 3254 (2014).
55. Y. Zhuang, J. G. Seong, Y. S. Do, W. H. Lee, M. J. Lee, M. D. Guiver, and Y. M. Lee, J. Membr. Sci. **504**, 55 (2016).
56. X. Ma, R. Swaidan, Y. Belmabkhout, Y. Zhu, E. Litwiller, M. Jouiad, I. Pinnau, and Y. Han, Macromolecules **45**, 3841 (2012).
57. S. Li, H. J. Jo, S. H. Han, C. H. Park, S. Kim, P. M. Budd, and Y. M. Lee, J. Membr. Sci. **434**, 137 (2013).
58. Y. J. Cho and H. B. Park, Macromol. Rapid Commun. **32**, 579 (2011).
59. F. Alghunaimi, B. Ghanem, N. Alaslai, R. Swaidan, E. Litwiller, and I. Pinnau, J. Membr. Sci. **490**, 321 (2015).
60. A. A. Shamsabadi, F. Seidi, M. Nozari, and M. Soroush, ChemSusChem **11**, 472 (2018).
61. C. M. Zimmerman and W. J. Koros, Polymer **40**, 5655 (1999).
62. C. M. Zimmerman and W. J. Koros, J. Polym. Sci., Polym. Phys. Ed. **37**, 1235 (1999).
63. R. L. Burns and W. J. Koros, Macromolecules **36**, 2374 (2003).
64. J. L. Santiago-Garcia, C. Alvarez, F. Sanchez, and G. Jose, J. Membr. Sci. **476**, 442 (2015).
65. S. Fu, E. S. Sanders, S. S. Kulkarni, and W. J. Koros, J. Membr. Sci. **487**, 60 (2015).
66. A. A. Kuznetsov, A. Yu. Tsegel'skaya, A. M. Orlova, N. A. Belov, S. V. Chirkov, R. Yu. Nikiforov, and A. Yu. Alentiev, Membr. Membr. Technol. **1**, 316 (2019).
67. M. Calle, A. E. Lozano, J. de Abajo, G. José, and C. Álvarez, J. Membr. Sci. **365**, 145 (2010).
68. C. Álvarez, A. E. Lozano, and G. José, J. Membr. Sci. **501**, 191 (2016).
69. M. Calle, C. García, A. E. Lozano, G. Jose, J. de Abajo, and C. Álvarez, J. Membr. Sci. **434**, 121 (2013).
70. T. Li, J. Liu, S. Zhao, Z. Chen, H. Huang, R. Guo, and Y. Chen, J. Membr. Sci. **585**, 282 (2019).
71. E. C. Mancilla, H. Hernández-Martinez, M. G. Zolotukhin, F. A. Ruiz-Treviño, M. O. González-Diaz, J. Cardenas, and U. Scherf, Ind. Eng. Chem. Res. **58**, 15280 (2019).
72. B. M. Lee, D. J. Kim, and S. Y. Nam, J. Nanosci. Nanotechnol. **15**, 2351 (2015).
73. *Membrane Materials for Gas and Vapor Separation. Synthesis and Application of Silicon-Containing Polymers,* Ed. by Yu. Yampolskii and E. Finkelshtein (Wiley, Chichester, 2017).
74. S. K. Sen and S. Banerjee, RSC Adv. **2**, 6274 (2012).
75. R. Chatterjee, S. Bisoi, A. G. Kumar, V. Padmanabhan, and S. Banerjee, ACS Omega **3**, 13510 (2018).
76. A. Dutta, A. Bisoi, R. Mukherjee, and R. Chatterjee, R. K. Das, and S. Banerjee, J. Appl. Polym. Sci. **135**, 46658 (2018).
77. S. Ghosh and S. Banerjee, J. Membr. Sci. **479**, 172 (2016).
78. P. Bandyopadhyay, D. Bera, S. Ghosh, and S. Banerjee, J. Membr. Sci. **447**, 413 (2013).
79. D. Bera, V. Padmanabhan, and S. Banerjee, Macromolecules **48** (13), 4541 (2015).
80. I. Ronova, A. Alentiev, and M. Bruma, Int. J. Eng. Res. Ind. Appl. **8** (12), 42 (2018).

Translated by T. Soboleva